Layered double hydroxides-silver-chlorin e6 nanocomposite for photo-chemo combination therapy to efficiently combat both Gram-positive and Gram-negative bacteria

Layered double hydroxides-silver-chlorin e6 nanocomposite for photo-chemo combination therapy to efficiently combat both Gram-positive and Gram-negative bacteria

Li Yan,[a,b,†,] Juan Li,[a,†] Ashna Gopal,[c] Samuel C. Roberts,[c] Jia-fu Lin,[a,*] Ting-ting Liu,[a] Tasnim Munshi,[d] Xiujuan Zhang,[e] and Xianfeng Chen[c,*]*

[a.] Antibiotics Research and Re-evaluation Key Laboratory of Sichuan Province, Sichuan Industrial Institute of Antibiotics (SIIA), Chengdu University, Sichuan 610052, P.R. China.
[b.] College of Health Science and Environmental Engineering, Shenzhen Technology University, Guangdong 518118, P.R. China.
[c.] School of Engineering, Institute for Bioengineering, The University of Edinburgh, King's Buildings, Mayfield Road, Edinburgh EH9 3JL, United Kingdom.
[d.] School of Chemistry, University of Lincoln, Brayford Pool, Lincoln, Lincolnshire, LN6 7TS, UK.
[e.] Jiangsu Key Laboratory for Carbon-Based Functional Materials & Devices, Institute of Functional Nano & Soft Materials (FUNSOM), Joint International Research Laboratory of Carbon-Based Functional Materials and Devices, Soochow University, Suzhou, Jiangsu 215123, P.R. China.

† Equal Contribution

[*] Corresponding authors
E-mail: xianfeng.chen@oxon.org or Michael.Chen@ed.ac.uk (X. Chen)
E-mail: yanli@sztu.edu.cn or tony_yan8@hotmail.com (L. Yan)
E-mail: linjiafu@cdu.edu.cn (J.F. Lin)

Keywords: Nanocomposite; Antimicrobial; Antibacterial; Photo-chemo combination therapy; Layered double hydroxides

Abstract: Antibiotics play an important role in the treatment of infectious diseases. However, the growing threat of drug-resistant bacteria has limited the availability and effectiveness of antibiotics. Here, we introduced an antibiotic nanocomposite using biocompatible and biodegradable layered double hydroxides as a matrix, followed by covalent conjugation of a photosensitizer, chlorin e6 (Ce6), and in-situ doping of silver nanoparticles for synergistic photo-chemo combination therapy to effectively kill both Gram-positive and Gram-negative bacteria. This layered double hydroxides-silver-chlorin e6 nanocomposite could be potentially utilized for treating various bacterial infections and overcoming bacterial resistance.

1. Introduction

The discovery of antibiotics revolutionized the treatment of infectious diseases and significantly improved human healthcare. [1-2] Among them, antibiotics which can kill a range of bacteria are extremely valuable in fighting infections when patients are in emergency situations or when doctors are unable to rapidly identify the specific bacteria causing the disease. [3] Additionally, such antibiotics can be used to treat drug-resistant bacteria that show low susceptibility to narrow-spectrum antibiotics. Due to their efficacy in these situations, nanoparticle-based antimicrobial systems have attracted tremendous interest owing to their unique advantages, including increased localization to bacteria, modulated interactions between drug and bacteria, and convenient incorporation of different approaches to synergistically fight antibiotic resistance.[4-9] For example, silver nanoparticles (AgNPs) have been widely demonstrated to display high efficiency against a range of bacteria.[10-12] However, practical applications of AgNPs are strictly hampered by their tendency to aggregate, which results in the loss of antibacterial activity. Indeed, it has been found that bacteria can develop resistance to AgNPs through the production of an adhesive flagellum protein, flagellin, which triggers AgNP aggregation.[13] Beyond antibiotic chemotherapy, photodynamic inactivation is a broadly considered an alternative approach to treat bacteria. In photodynamic inactivation, photosensitizers can generate singlet oxygen ($^1O_2$), which fatally damages bacteria/cells through disruption of DNA and membrane structures.[14-16] For instance, chlorin e6 (Ce6) has been used to treat Gram-positive and Gram-negative bacteria. However, the low photostability of Ce6 makes it lose its capacity to generate singlet oxygen rapidly under light exposure.

To address these problems, we designed a system made up of a biocompatible and biodegradable, positively charged layered double hydroxide (LDH) nanosheets,[17-24] doped with AgNPs and Ce6. Ce6 is incorporated to achieve a synergistic antibacterial effect together with AgNPs. The cationic charge of LDH nanosheets can physically disrupt the bacterial

membrane and improve membrane translocation. AgNPs are doped onto LDH nanosheets to improve their sustained antibacterial activity by preventing aggregation. Additionally, Ce6 molecules are covalently conjugated to the LDH nanosheets to prevent quenching and to improve their photostability, consequently maintaining a high capacity of singlet oxygen generation to effectively kill bacteria. With this integrated design, we prepared a LDH-silver-Ce6 nanocomposite, characterized its properties, and tested its efficacy in treating Gram-positive bacteria (*S. aureus*), Gram-negative bacteria (*Escherichia coli* (*E. coli*) and Pseudomonas aeruginosa (*P. aeruginosa*)), and the multi-drug-resistant bacterium methicillin-resistant *Staphylococcus aureus* (MRSA). *P. aeruginosa* is commonly implicated in healthcare-associated infections and is resistant to many antibiotics. MRSA is listed by the World Health Organization (WHO) as one of the antibiotic-resistant "priority pathogens."[25] Overall, our work demonstrated that the LDH-silver-Ce6 nanocomposite is able to effectively inhibit the growth of Gram-positive and Gram-negative bacteria.

2. Results and discussion

The overall synthesis procedures are presented in **Figure 1**. LDH nanosheets were synthesized using the co-precipitation method with and without sodium dodecyl sulfate (SDS). (Figure S1a) The powder X-ray diffraction (XRD) pattern indicates that when SDS was added to the reaction, the (003) peak of LDH nanosheets shifts from 11.5° (in the absence of SDS) to 3.4°, suggesting a large spacing of 26 Å. (Figure S1b) Subsequently, APTES-conjugated photosensitizer Ce6 molecules were covalently bonded to LDH nanosheets in the presence of cetyltrimethylammonium bromide (CTAB). The role of CTAB is to extract SDS molecules from the gallery between LDH layers. As shown in Figure S2, there is a broad peak at 1000-1200 cm^{-1} in the Fourier transform infrared (FTIR) spectrum, indicating the Si−O−Si asymmetric stretching vibration, suggesting bond formation between LDH and APTES. After Ce6 conjugation, $AgNO_3$ was reacted with LDH nanosheets to yield AgNP-doped LDH nanocomposites. (**Figure 2**a-b) The XRD pattern demonstrates that the fabricated AgNP-

doped nanocomposite possesses the same peaks as those of LDH nanosheets. (Figure 2c) The average particle size of LDH nanosheets is approximately 50 nm. To further demonstrate successful doping of AgNPs to LDH nanosheets, X-ray photoelectron spectroscopy (XPS) was conducted. (Figure 2d-e) From the XPS spectrum, it is clear that Mg, C, Ag, O, Si, and Al elements are present in the fabricated nanomaterials. The spectrum of Ag 3d (Figure 2e) at approximately 268.1 eV can be ascribed to metallic silver. In addition, the lattice distance of AgNPs measured in the high-resolution transmission electron microscopy (HRTEM) image is approximately 0.23 nm, corresponding to the (111) cubic phase of silver metal. (Figure 2b)

After preparation of the nanocomposite, its properties, photostability, and reactive-oxygen-species-generation capacity were evaluated. (**Figure 3**) Figure 3a shows that the absorption spectrum of the AgNP-doped LDH-Ce6 nanocomposite is very similar to that of free Ce6 molecules. Then, the photostability of the AgNP-doped LDH-Ce6 nanocomposite (Figure 3b) was evaluated and compared with that of free Ce6 molecules. (Figure 3c) Upon light exposure, a significant decrease in the absorbance intensity of free Ce6 molecules can be observed (Figure 3c), indicating the poor photostability of the Ce6 molecules. In contrast, the photostability of the AgNP-doped LDH-Ce6 nanocomposite is much greater, shown by the slower rate of decrease in absorbance intensity. (Figure 3b) For example, after 10 min light irradiation, over 80% of the absorbance intensity of AgNP-doped LDH-Ce6 nanocomposite remains, while there is less than 30% of that of free Ce6 molecules remaining. (Figure 3d) This means that the LDH nanocomposite can effectively protect Ce6 molecules from photobleaching. Following this, the ability of the nanocomposite to generate $^1O_2$ was evaluated using 1,3-diphenylisobenzofuran (DPBF) as a chemical probe. DPBF molecules have a highly specific reactivity towards $^1O_2$, which leads to a decrease in absorbance intensity. On addition of AgNP-doped LDH-Ce6 nanocomposites and free Ce6 molecules, the absorbance of DPBF quickly drops, indicating successful generation of $^1O_2$. (Figure 3e) To evaluate the photostability and $^1O_2$ generation capacity of the AgNP-doped LDH-Ce6

nanocomposites and free Ce6 molecules, both materials were illuminated for 30 min and then the generation of $^1O_2$ generation was measured. It was found that free Ce6 molecules completely lost their capacity to generate $^1O_2$; in contrast, the AgNP-doped LDH-Ce6 nanocomposite retained its capacity to effectively generate $^1O_2$. (Figure 3f) Overall, these results reveal that the photostability of the AgNP-doped LDH-Ce6 nanocomposite is significantly increased compared to that of free Ce6 molecules.

After demonstrating excellent photostability and $^1O_2$-generation capacity, the antibacterial performance of AgNP-doped LDH-Ce6 nanocomposites was evaluated using Gram-negative *E. coli* and *P. aeruginosa*, Gram-positive *S. aureus*, and MRSA. (**Figure 4** and Figure S3-S6) First, the possibility that bacterial inhibition was due to light irradiation or the LDH nano-carrier in the delivery system was excluded. From the results, it was found that the intensity of the light irradiation used in these experiments did not hinder the growth of any of the groups of bacteria and that LDH nanosheet vehicles demonstrated negligible bacterial inhibition. (Figure S7) However, under light illumination, 32 μg/mL AgNP-doped LDH-Ce6 nanocomposites containing 0.432 μg/mL and 2.24 μg/mL of AgNPs and Ce6, respectively, could inhibit Gram-positive bacteria (*S. aureus*) and MRSA but could not inhibit growth of Gram-negative bacteria (*E. coli* and *P. aeruginosa*). When the concentration increased to 160 μg/mL with 2.16 μg/mL and 11.2 μg/mL of AgNPs and Ce6, respectively, the material began to fully inhibit the growth of both Gram-negative bacteria (*E. coli* and *P. aeruginosa*), Gram-positive bacteria (*S. aureus*), and MRSA when illuminated by light. In contrast, without illumination, the four strains of bacteria still grew well keeping other conditions the same. (Figure 4b, e, h, k) This phenomenon indicates that in addition to the AgNPs, the loaded Ce6 also acts to effectively inhibit bacterial growth. As the concentration was further increased to 800 μg/mL, with 10.8 μg/mL and 56 μg/mL of AgNPs and Ce6, respectively, the material could fully inhibit the growth of all Gram-negative and Gram-positive bacteria tested even without light illumination. In sharp contrast, 10.8 μg/mL of AgNPs alone cannot effectively

inhibit the growth of E. *coli* and P. *aeruginosa* and S. *aureus*. (Figure S8) These observations reveal the synergistic effect of AgNPs and Ce6 in killing bacteria. Overall, these results collectively demonstrate that AgNP-doped LDH-Ce6 nanocomposites can effectively inhibit a spectrum of bacteria including MRSA, one of the most drug-resistant super-bacteria.

Finally, to prove that singlet oxygen generation is responsible for inhibition of bacteria growth, we used CellRox® Orange as a fluorogenic probe to detect generated singlet oxygen in bacteria. CellRox® Orange is non-fluorescent but becomes fluorescent in the presence of ROS. From **Figure 5**, it can be seen that negligible fluorescence signals of CellRox® Orange can be found in the untreated group (Control), the 650 nm LED-irradiated group, and the heat-killed group, indicating negligible generation of ROS. In great contrast, ROS was clearly detected in AgNP-doped-LDH-Ce6-nanocomposite-treated groups. It is worth noting that, when bacteria were treated with AgNP-doped LDH-Ce6 nanocomposites in the presence of LED irradiation, a stronger ROS signal was detected. This phenomenon demonstrates that the nanocomposite is able to effectively generate singlet oxygen for bacterial killing.

3. Conclusions

In summary, we have developed a photo-excited AgNP-doped LDH-Ce6 nanocomposite to effectively combat a spectrum of bacteria. By incorporating AgNPs and Ce6 to the LDH nanocarrier, this antibacterial system demonstrates enhanced the photostability of Ce6 and the antibacterial activity of AgNPs as well as possesses sustained ROS-generation capacity. With these superior properties, the antibacterial system exhibits significant efficacy against bacteria including Gram-positive, Gram-negative, and drug resistant bacteria.

4. Experimental Section

4.1 Chemicals and Characterization: Sodium hydroxide, aluminium chloride, hexadecyl trimethyl ammonium bromide (CTAB), dimethyl sulfoxide (DMSO), magnesium chloride dehydrate, and dichloromethane were obtained from Kelong Chemical. Sodium dodecyl sulfate (SDS), 1-ethyl-3-(3-dimethylaminopropyl) carbodiimide (EDC), ethyl alcohol, 1,3-Diphenylisobenzofuran (DPBF), and

silver nitrate were purchased from Damas-beta Chemical. Ampicillin and Polymyxin B were bought from Solarbio. Silver nanoparticles with 10 nm size were purchased from STREM Chemical. (3-aminopropyl) triethoxysilane (APTES) and chlorin e6 (Ce6) were purchased from J&K and Frontier Scientific, respectively. 96-well cell culture plates, cell culture dishes, and centrifuge tubes were obtained from Corning. Transmission electron microscopy (TEM) images were taken on a Tecnai G2 F20 S-TWIN. The UV−vis absorption was determined with a UV-1900PC UV−visible spectrophotometer. Powder X-ray diffraction (XRD) patterns, Fourier transform infrared spectroscopy (FT-IR), and X-ray photoelectron spectroscopy (XPS) were recorded on a BRUCKER D8 instrument using Cu Kα radiation, a Nicolet IS10, and a Thermo ESCALAB 250Xi, respectively.

4.2 Preparation of LDH-SDS Nanoparticles: First, 0.2307 g of sodium dodecyl sulfate was added into 16 mL of 0.15 mol/L NaOH solution under active stirring. Second, 4 mL of solution containing 0.2 mol/L $MgCl_2$ and 0.1 mol/L $AlCl_3$ was added and stirred for 10 min. Third, the solution was centrifuged at 4000 rpm for 5 min and the sediment was washed with water three times, followed by re-dispersing in 16 mL of water and incubation at 80 ºC for 24 h. Finally, the product was collected by centrifugation and freeze-drying.

4.3 Preparation of APTES-Conjugated Ce6: 3.5 mg of Ce6 and 50 μL of APTES were added into 2 mL of dichloromethane in presence of EDC as a catalyst for 24 h. The loading of Ce6 was calculated by UV-Absorption measurement.

4.4 Preparation of AgNP-Doped LDH-Ce6 Nanocomposite: First, 100 mg of CTAB was dissolved into 10 mL of dichloromethane. Second, 100 mg of LDH-SDS and APTES-conjugated Ce6 were added into the solution. Third, the solution was sonicated for 30 min and stirred for 24 h. After the reaction, the product was washed with dichloromethane, ethyl alcohol and water three times and re-dispersed in 15 mL water. Fourth, 100 μL of 0.1 M $AgNO_3$ was added into the solution and stirred at 100 ºC for 4 h. Finally, the product was washed with water three times. The loading of AgNPs was calculated by XPS analysis.

4.5 Analysis of Singlet Oxygen Generation Capacity: Briefly, 3 mL of 0.05 mg/mL DPBF solution in DMSO was added into a quartz cell. Free Ce6 or LDH-Ce6, containing the same amount of Ce6 (0.9 μg), was added. The quartz cell was irradiated using a 650 nm LED lamp. After irradiation for different time intervals, the absorbance of each cell was measured at 410 nm.

4.6 Antibacterial Test: *Escherichia coli* (*E. coli*), *Staphylococcus aureus* (*S. aureus*), *Pseudomonas aeruginosa* (*P. aeruginosa*), and MRSA were selected as model bacteria to evaluate the antibacterial activity. The bacterial concentration in lysogeny broth (LB) was approximately 10^6 CFU mL^{-1}, and the bacteria were cultured at 37 ^oC. Corning 96-well plates were utilized for this test. In the light treatment group, the Corning 96-well plates were exposed to 650 nm LED light for 30 min after 2 h incubation. The bacterial growth curve was determined by measuring the optical density at 600 nm.

5.7 ROS staining of E. *coli*: A single colony of *E. coli* (ATCC25922) was inoculated into 10 mL of LB and grown overnight at 37 °C. The culture was diluted to OD_{595} 0.1 and incubated until mid-log phase. The culture was washed in PBS and the optical density was adjusted to 0.05 (~10^6 CFU mL^{-1}). Aliquots remained untreated, heat-killed (65 °C; 30 min), or were incubated with 16 μg mL^{-1} LDH-silver-Ce6 nanocomposites for 2h at 37 °C. Where appropriate, 5 μM CellRox Orange (ThermoFisher) was added to the aliquots for the final hour of incubation. Aliquots were irradiated by the 650 nm LED as necessary for 30 min. Samples were serially diluted for CFU plating. The aliquots that had been incubated with CellRox Orange were counterstained with 5 μM Syto60 (ThermoFisher). Following washing in PBS, bacterial cells were loaded into poly-d-lysine-coated 8-well chambers (IBIDI) for confocal laser scanning microscopy (Leica, SP8). CellRox Orange/Syto60 images were obtained with excitation 543 nm (collection 550-620 nm) and 633 nm (collection 640-700 nm), respectively. Image brightness and contrast was enhanced using proprietary software.

Acknowledgements

The authors acknowledge the support provided from National Natural Science Foundation of China (No. 81803480, 2167315, 11811530640), the Chengdu University (No. 2081916010), School of Engineering of The University of Edinburgh, and the Royal Society Research Grant Scheme RG150564. L. Yan and J. Li contributed equally to this work.

References

1 I. Levin-Reisman, I. Ronin, O. Gefen, I. Braniss, N. Shoresh and N. Q. Balaban, Antibiotic tolerance facilitates the evolution of resistance. *Science*, **2017**, 355, 826-830.

2 M. S. Butler, M. A. T. Blaskovich and M. A. Cooper, Antibiotics in the clinical pipeline at the end of 2015. *J. Antibiot*., **2017**, 70, 3-24.

3 M. F. Richter, B. S. Drown, A. P. Riley, A. Garcia, T. Shirai, R. L. Svec and P. J. Hergenrother, Predictive compound accumulation rules yield a broad-spectrum antibiotic. *Nature*, **2017**, 545, 299-304.

4 C. Mao, Y. Xiang, X. Liu, Z. Cui, X. Yang, K. W. K. Yeung, H. Pan, X. Wang, P. K. Chu and S. Wu, Photo-Inspired Antibacterial Activity and Wound Healing Acceleration by Hydrogel Embedded with Ag/Ag@AgCl/ZnO Nanostructures. *ACS Nano*, **2017**, 11, 9010-9021.

5 G. Hu, B. Song, A. Jiang, B. Chu, X. Shen, J. Tang, Y. Su and Y. He, Multifunctional Silicon–Carbon Nanohybrids Simultaneously Featuring Bright Fluorescence, High Antibacterial and Wound Healing Activity. *Small*, **2019**, 1803200.

6 H. Song, Y. Ahmad Nor, M. Yu, Y. Yang, J. Zhang, H. Zhang, C. Xu, N. Mitter and C. Yu, Silica Nanopollens Enhance Adhesion for Long-Term Bacterial Inhibition. *J. Am. Chem. Soc.*, **2016**, 138, 6455−6462.

7 X. Yang, J. Yang, L. Wang, B. Ran, Y. Jia, L. Zhang, G. Yang, H. Shao and X. Jiang, Pharmaceutical Intermediate-Modified Gold Nanoparticles: Against Multidrug-Resistant Bacteria and Wound-Healing Application via an Electrospun Scaffold. *ACS Nano*, **2017**, 11, 5737-5745.

8 D. Mao, F. Hu, Kenry, S. Ji, W. Wu, D. Ding, D. Kong and B. Liu, Metal–Organic-Framework-Assisted In Vivo Bacterial Metabolic Labeling and Precise Antibacterial Therapy. *Adv. Mater*., **2018**, 30, 201706831.

9 J. F. Lin, J. Li, A. Gopal, T. Munshi, Y. W. Chu, J. X. Wang, T. T. Liu, B. Shi, X. Chen and L. Yan, Synthesis of photo-excited Chlorin e6 conjugated silica nanoparticles for enhanced

anti-bacterial efficiency to overcome methicillin-resistant Staphylococcus aureus. *Chem. Commun.*, **2019**, 18, 2656-2659.

10 M. Lv, S. Su, Y. He, Q. Huang, W. Hu, D. Li, C. Fan and S.T. Lee, Long-term antimicrobial effect of silicon nanowires decorated with silver nanoparticles. *Adv. Mater.* **2010**, 22, 5463-5467.

11 M. Zhang, Y. Zhao, L. Yan, R. Peltier, W. Hui, X. Yao, Y. Cui, X. Chen, H. Sun and Z. Wang, Interfacial Engineering of Bimetallic Ag/Pt Nanoparticles on Reduced Graphene Oxide Matrix for Enhanced Antimicrobial Activity. *ACS Appl. Mater. Interfaces*, **2016**, 8, 8834−8840.

12 A. Gao, R. Hang, X. Huang, L, Zhao, X. Zhang, L. Wang, B. Tang, S. Ma and P. K. Chu, The effects of titania nanotubes with embedded silver oxide nanoparticles on bacteria and osteoblasts. *Biomaterials*, **2014**, 35, 4223−4235.

13 A. Panáček, L. Kvítek L, M. Smékalová, R. Večeřová, M. Kolář, M. Röderová, F. Dyčka, M. Šebela, R. Prucek, O. Tomanec O and R. Zbořil R, Bacterial resistance to silver nanoparticles and how to overcome it. *Nat. Nanotechnol*., **2018**, 13, 65–71.

14 M. Lan, S. Zhao, W. Liu, C.S. Lee, W. Zhang and P. Wang, Photosensitizers for Photodynamic Therapy. *Adv. Healthcare Mater.*, **2019**, 8, e1900132.

15 J. Wang, H. Wu, Y. Yang, R. Yan, Y. Zhao, Y. Wang, A. Chen, S. Shao, P. Jiang and Y. Q. Li, Bacterial species-identifiable magnetic nanosystems for early sepsis diagnosis and extracorporeal photodynamic blood disinfection. *Nanoscale*, **2018**, 10, 132-141.

16 G. B. Yang, L. G. Xu, Y. Chao, J. Xu, X. Q. Sun, Y. F. Wu, R. Peng and Z. Liu, Hollow MnO2 as a tumor-microenvironment-responsive biodegradable nano-platform for combination therapy favoring antitumor immune responses. *Nat. Commun*., **2017**, 8, 902.

17 H. Zuo, W. Chen, H. M. Cooper and Z. P. Xu, A Facile Way of Modifying Layered Double Hydroxide Nanoparticles with Targeting Ligand-Conjugated Albumin for Enhanced Delivery to Brain Tumour Cells. *ACS Appl. Mater. Interfaces*, **2017**, 9, 20444-20453.

18 N. Mitter, E. A. Worrall, K. E. Robinson, P. Li, R. G. Jain, C. Taochy, S. J. Fletcher, B. J. Carroll, G. Q. Lu and Z. P. Xu, Clay nanosheets for topical delivery of RNAi for sustained protection against plant viruses. *Nat. Plants*, **2017**, 3, 16207.

19 B. Li, Z. Gu, N. Kurniawan, W. Chen and Z. P. Xu, Manganese-Based Layered Double Hydroxide Nanoparticles as a T1-MRI Contrast Agent with Ultrasensitive pH Response and High Relaxivity. *Adv. Mater*., **2017**, 29, 1700373.

20 L. Yan, M. Zhou, X. Zhang, L. Huang, W. Chen, V. A. L. Roy, W. Zhang and X. F. Chen, A Novel Type of Aqueous Dispersible Ultrathin-Layered Double Hydroxide Nanosheets for in Vivo Bioimaging and Drug Delivery. *ACS Appl. Mater. Interfaces*, 2017, 9, 34185-34193.

21 N. Wang, Z. G. Wang, Z. F. Xu, X. F. Chen and G. Y. Zhu, A Cisplatin-Loaded Immunochemotherapeutic Nanohybrid Bearing Immune Checkpoint Inhibitors for Enhanced Cervical Cancer Therapy. *Angew. Chem. Int. Ed.,* **2018**, 13, 3426-3430.

22 S. Mallakpour, M. Dinari and V. Behranvand, Ultrasonic-assisted synthesis and characterization of layered double hydroxides intercalated with bioactive N,N0-(pyromellitoyl)-bis-L-a-amino acids. *RSC Advances*, **2013**, 3, 23303-23308.

23 S. Mallakpour, M. Dinari and M. Hatami, Modification of Mg/Al-layered double hydroxide with L-aspartic acid containing dicarboxylic acid and its application in the enhancement of the thermal stability of chiral poly(amide-imide), *RCS Advances*, **2014**, 4, 42114.

24 S. Mallakpour, M. Dinari, Preparation and characterization of new organoclays using natural amino acids and Cloisite Na^+, *Applied Clay Sci.* **2011**,51, 353-359.

25 E. Tacconelli, E. Carrara, et al., Discovery, research, and development of new antibiotics: the WHO priority list of antibiotic-resistant bacteria and tuberculosis, *Lancet Infect. Dis.*, **2017**, 18, 318-327.

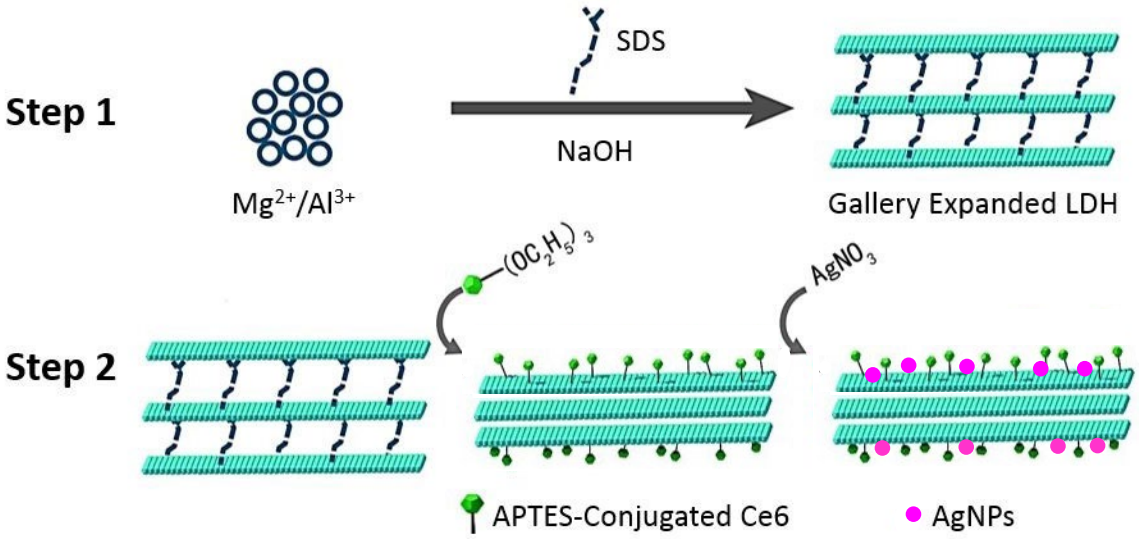

Figure 1. Schematic illustration of LDH-silver-Ce6 nanocomposite fabrication and photo-inspired disinfection. The LDH-silver-Ce6 nanocomposite is formed in two stages: Step 1. Fabrication of gallery expanded LDH nanoparticles and Step 2. Doping with Ce6 and AgNPs.

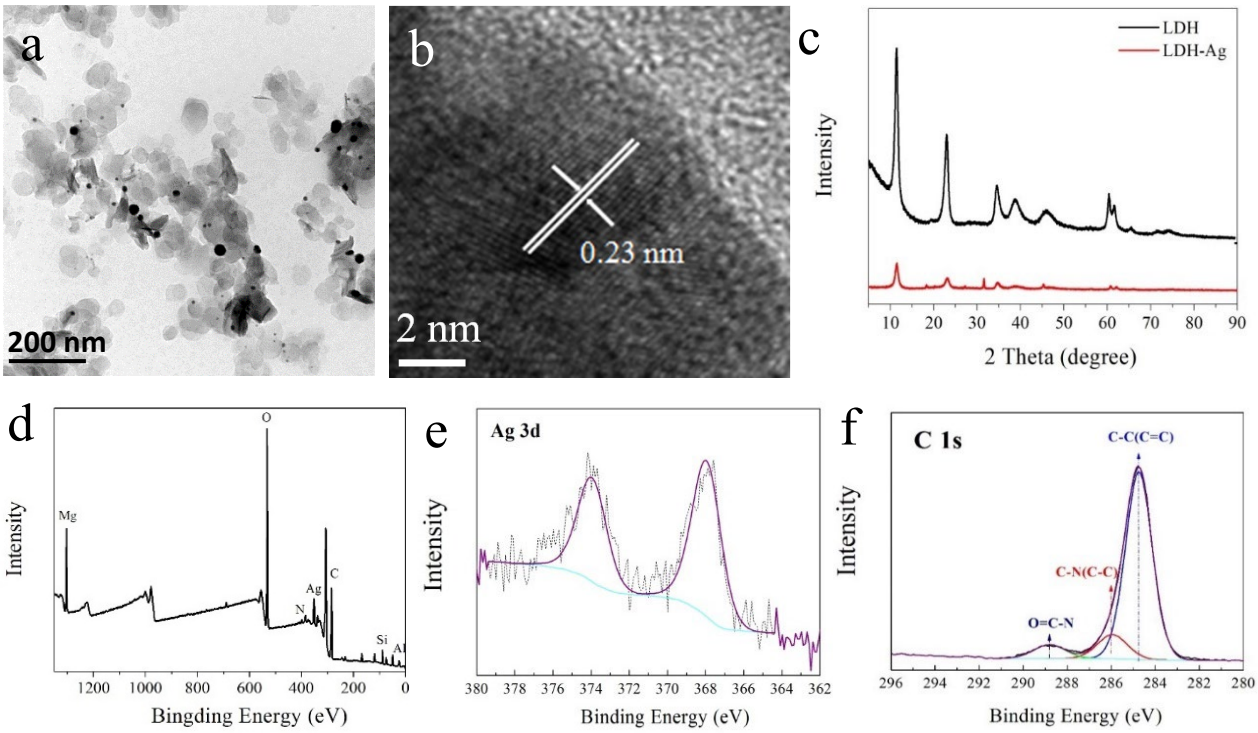

Figure 2. Characterization of AgNP-doped LDH-Ce6 nanocomposites. a. TEM image of the fabricated nanocomposite. b. HRTEM image of a silver nanoparticle. c. Powder XRD patterns of AgNP-doped LDH-Ce6 nanocomposites and conventional LDH. XPS spectra of AgNP-doped LDH-Ce6 nanocomposites: d. survey spectrum; e. Ag 3d spectrum; and f. C1s spectrum.

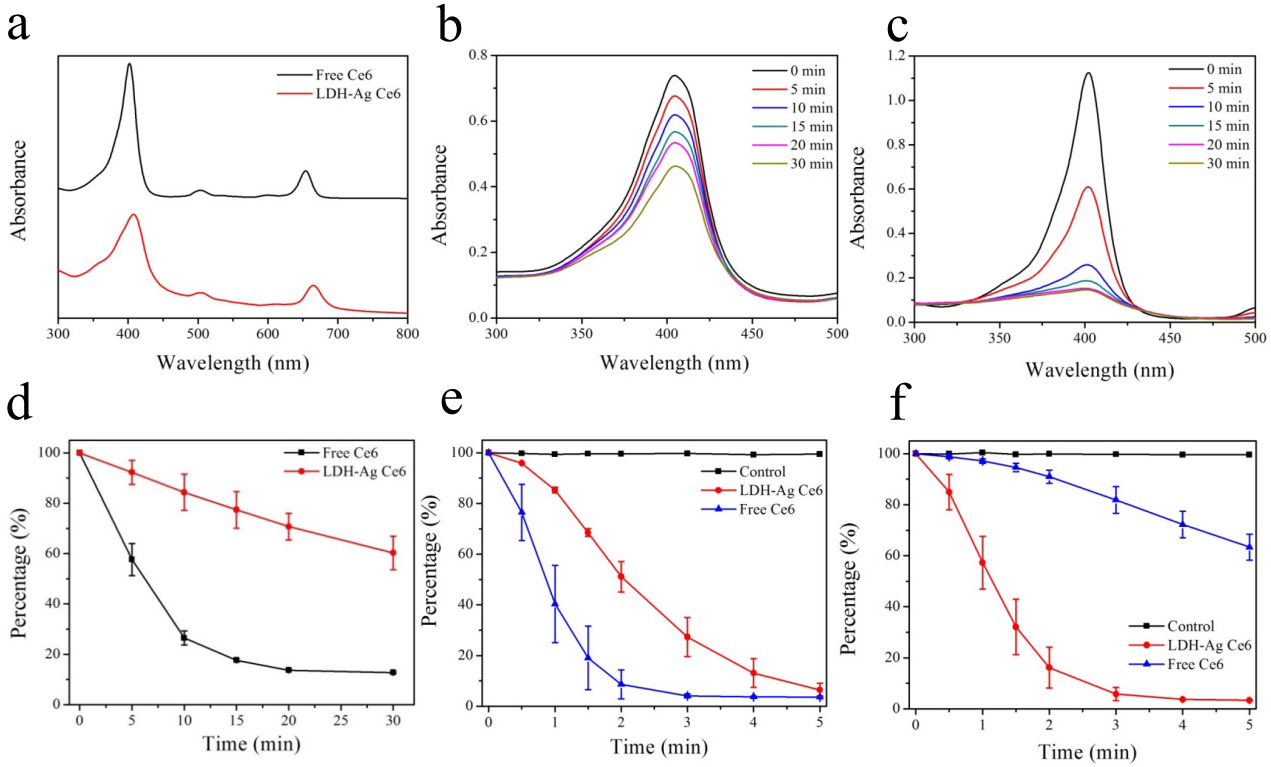

Figure 3 The optical properties and singlet oxygen generation capacity. a. Absorption spectra of the AgNP-doped LDH-Ce6 nanocomposite and free Ce6. **b, c.** Time-dependent absorbance change of **b.** AgNP-doped LDH-Ce6 nanocomposite, **c.** free Ce6, caused by 650 nm light irradiation. **D.,** Normalized absorbance intensity change of AgNP-doped LDH-Ce6 nanocomposite and free Ce6 (data from b, c). **e, f.** The absorbance of DPBF with the addition of the AgNP-doped LDH-Ce6 nanocomposite and free Ce6 under LED illumination. The control group is DPBF alone. **e.** DPBF was added with fresh AgNP-doped LDH-Ce6 nanocomposite and free Ce6, **f.** AgNP-doped LDH-Ce6 nanocomposite and free Ce6 were illuminated under 650 nm LED light irradiation for 0.5 h before adding to DPBF. Data in d-f are expressed as mean ± s.d. (indicated by error bar), based on values obtained from three replicates (n=3).

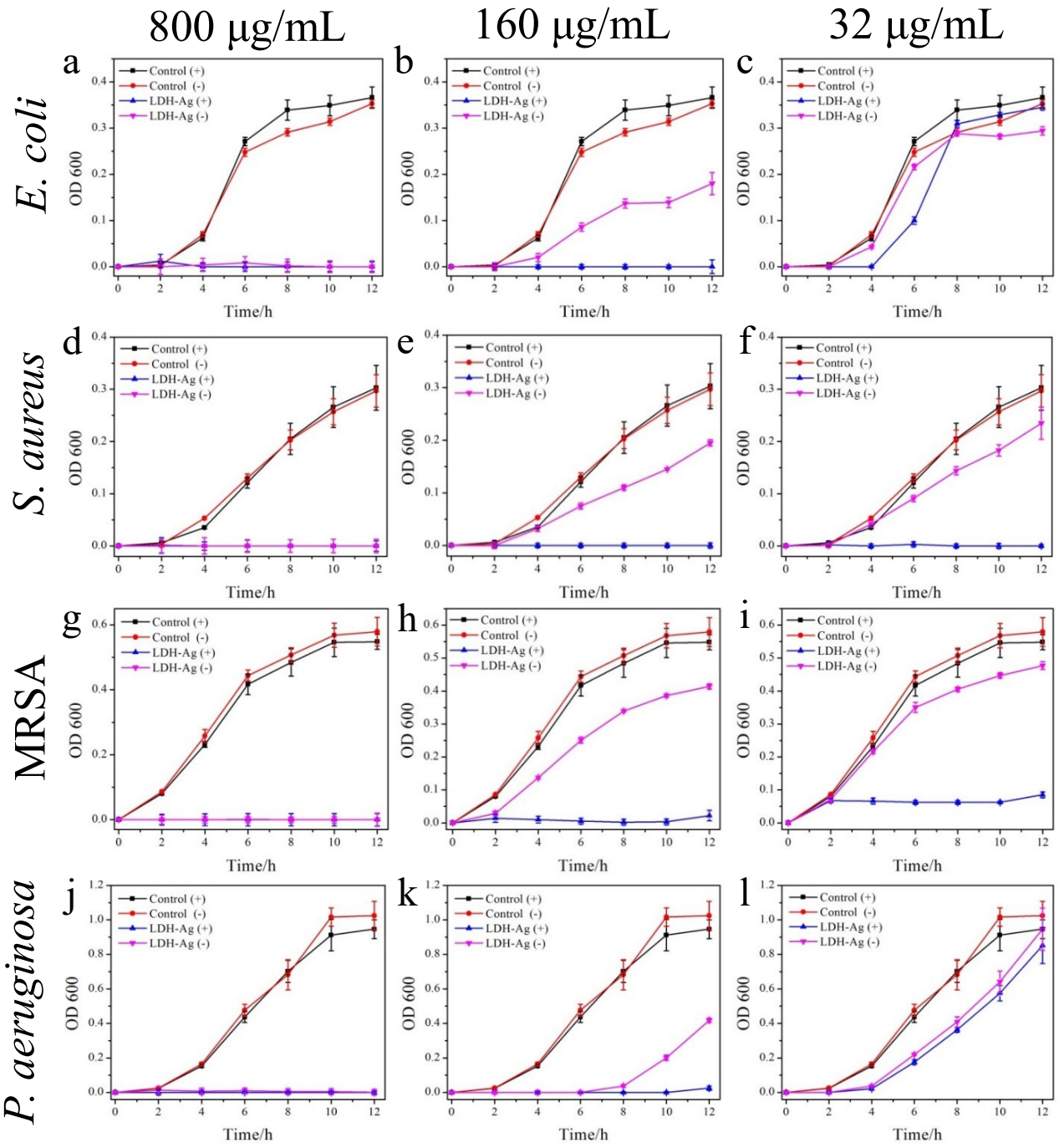

Figure 4. Bacterial inhibition analysis of AgNP-doped LDH-Ce6 nanocomposites. (a-c) *E. coli*, (d-f) *S aureus*, (g-i) MRSA and (j-l) *P. aeruginosa*. "+" indicates with light illumination; "-" indicates without light illumination. Control indicates bacteria only. All data are expressed as mean ± s.d. (indicated by error bar) based on values obtained from six biological replicates (n=6).

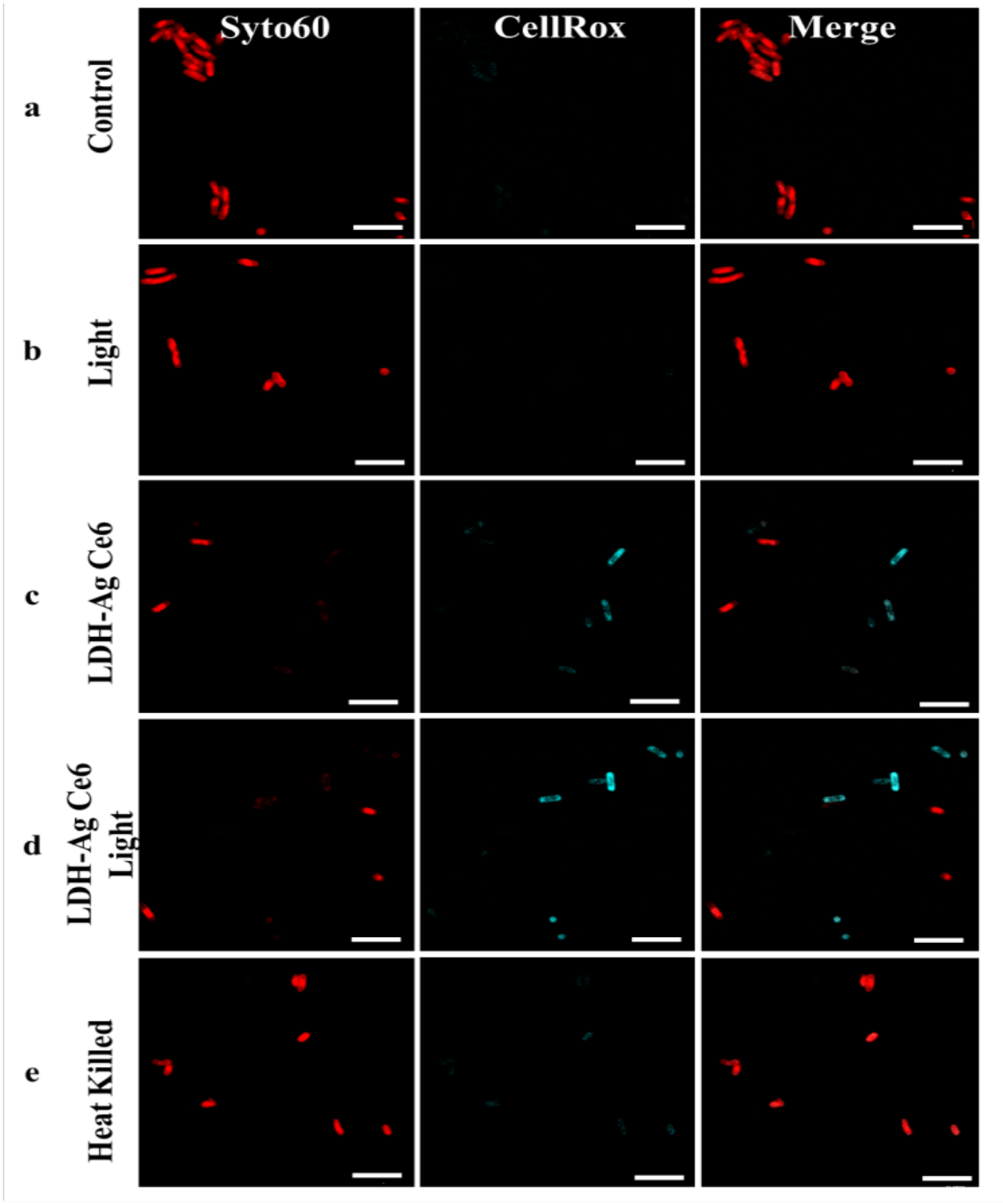

Figure 5. ROS generation of *E. coli* after different treatments. a. Untreated as control. b. Treated with LED light irradiation. c. Treated with AgNP-doped LDH-Ce6 nanocomposites. d. Treated with AgNP-doped LDH-Ce6 nanocomposites and light irradiation. e. Heat killed. Scale bars show 5µm.

Supporting Information

Layered double hydroxides-silver-chlorin e6 nanocomposite for photo-chemo combination therapy to efficiently combat both Gram-positive and Gram-negative bacteria

Li Yan,[a,b,†,] Juan Li,[a,†] Ashna Gopal,[c] Samuel C. Roberts,[c] Jia-fu Lin,[a,*] Ting-ting Liu,[a] Tasnim Munshi,[d] Xiu-juan Zhang,[e] and Xian-feng Chen[c,*]*

[a.] Antibiotics Research and Re-evaluation Key Laboratory of Sichuan Province, Sichuan Industrial Institute of Antibiotics (SIIA), Chengdu University, Sichuan 610052, P.R. China.
[b.] College of Health Science and Environmental Engineering, Shenzhen Technology University, Guangdong 518118, P.R. China.
[c.] School of Engineering, Institute for Bioengineering, The University of Edinburgh, King's Buildings, Mayfield Road, Edinburgh EH9 3JL, United Kingdom.
[d.] School of Chemistry, University of Lincoln, Brayford Pool, Lincoln, Lincolnshire, LN6 7TS, UK.
[e.] Jiangsu Key Laboratory for Carbon-Based Functional Materials & Devices, Institute of Functional Nano & Soft Materials (FUNSOM), Joint International Research Laboratory of Carbon-Based Functional Materials and Devices, Soochow University, Suzhou, Jiangsu 215123, P.R. China.

† Equal Contribution

[*] Corresponding authors
E-mail: xianfeng.chen@oxon.org or Michael.Chen@ed.ac.uk (X.F. Chen)
E-mail: yanli@sztu.edu.cn or tony_yan8@hotmail.com (L. Yan)
E-mail: linjiafu@cdu.edu.cn (J.F. Lin)

Keywords: Nanocomposite; Antimicrobial; Antibacterial; Photo-chemo combination therapy; Layered double hydroxides

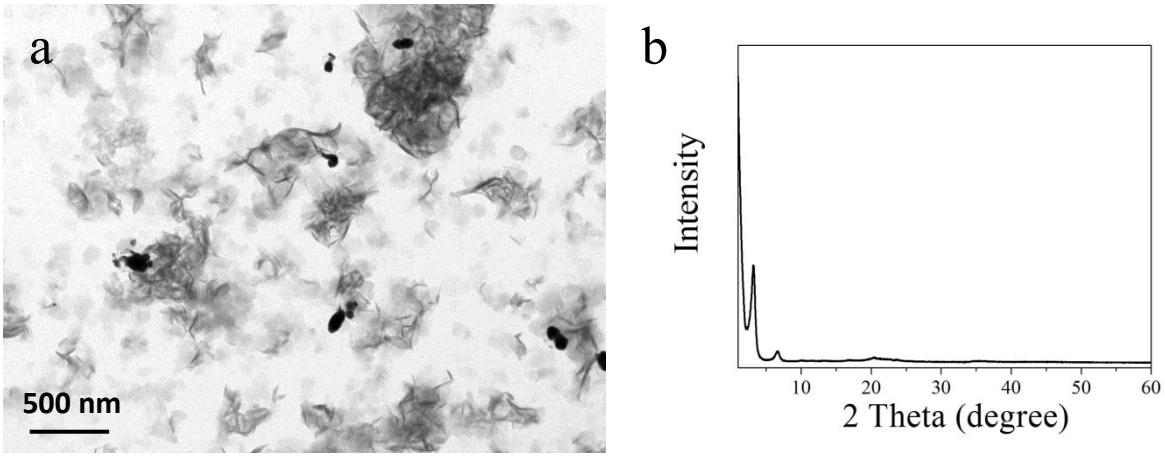

Figure S1. Characterization of gallery expanded LDH. a. TEM. b. Powder XRD pattern.

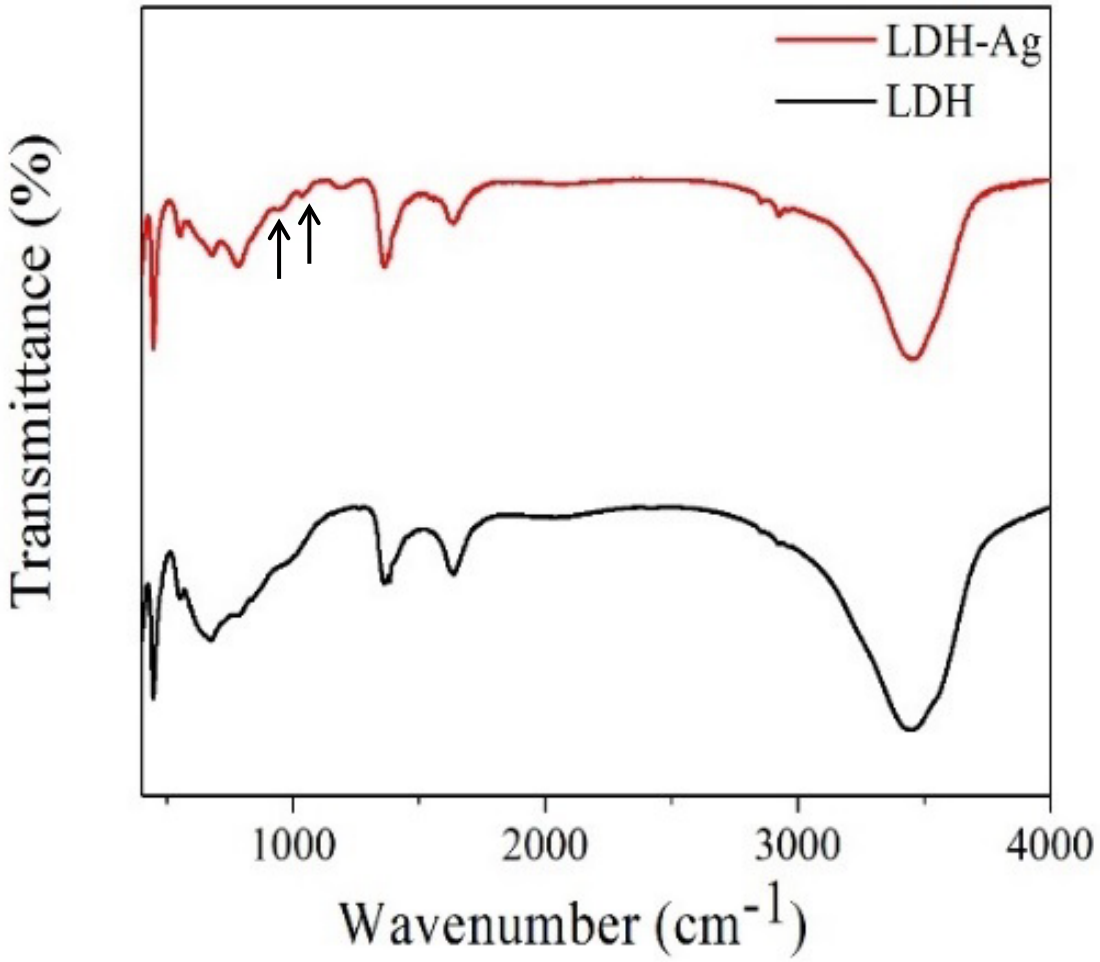

Figure S2. Fourier transform infrared spectroscopy of AgNP-doped LDH-Ce6 nanocomposites and conventional LDH nanoparticles. (The arrows indicat the Si−O−Si asymmetric stretching vibration, suggesting bond formation between LDH and APTES)

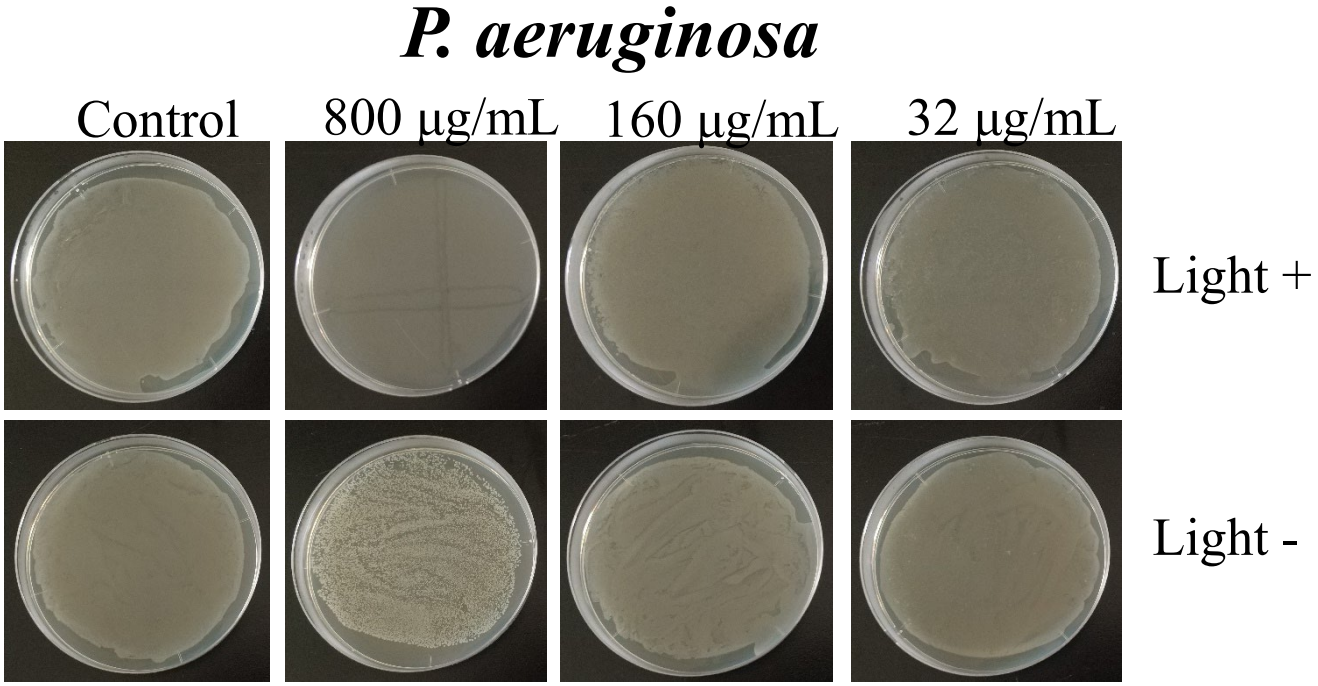

Figure S3. Photoscopic images of *P. aeruginosa*. Number of colony-forming units after treated with AgNP-doped LDH-Ce6 nanocomposites with and without light irradiation.

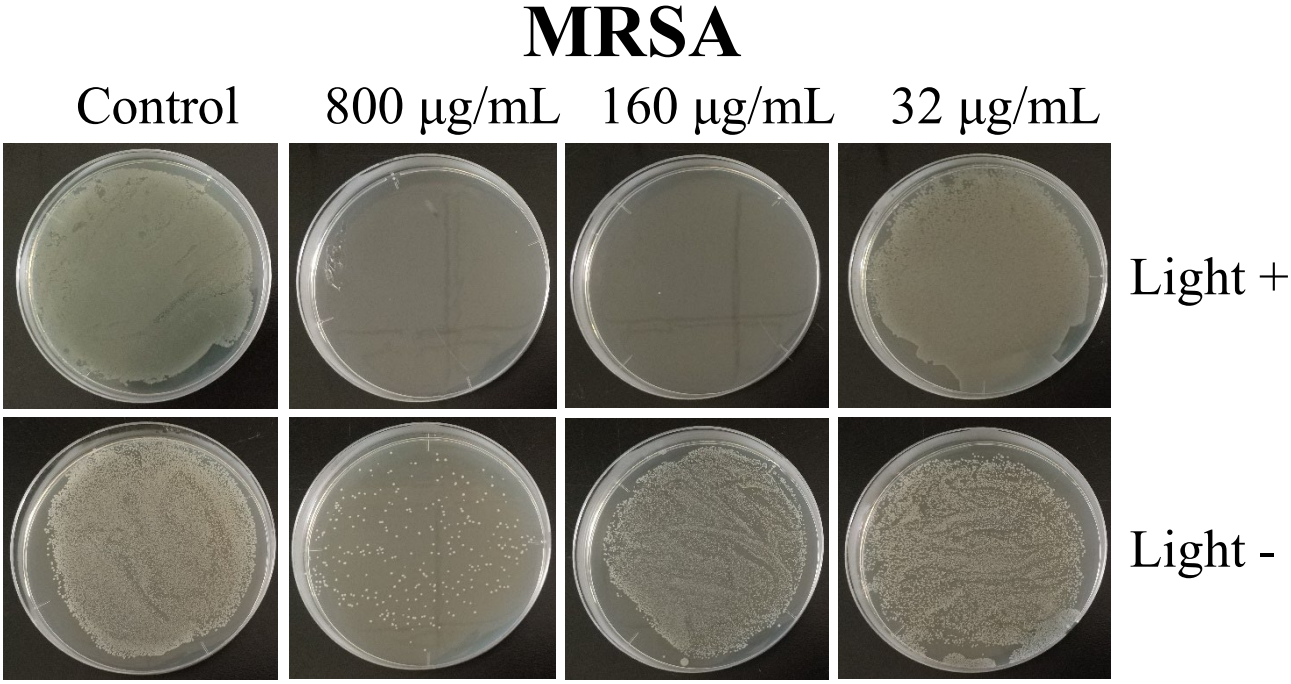

Figure S4. Photoscopic images of MRSA. Number of colony-forming units after treatment with AgNP-doped LDH-Ce6 nanocomposites with and without light irradiation.

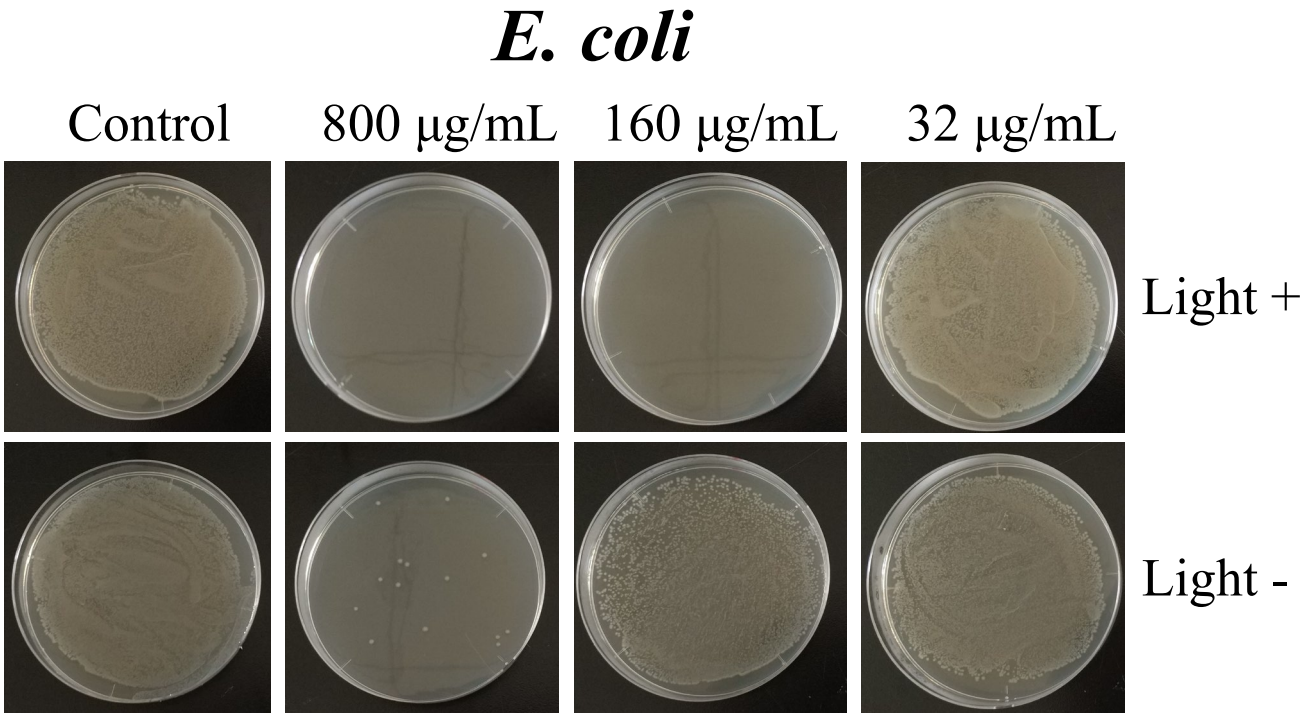

Figure S5. Photoscopic images of *E. coli.* Number of colony-forming units after treated with AgNP-doped LDH-Ce6 nanocomposites with and without light irradiation.

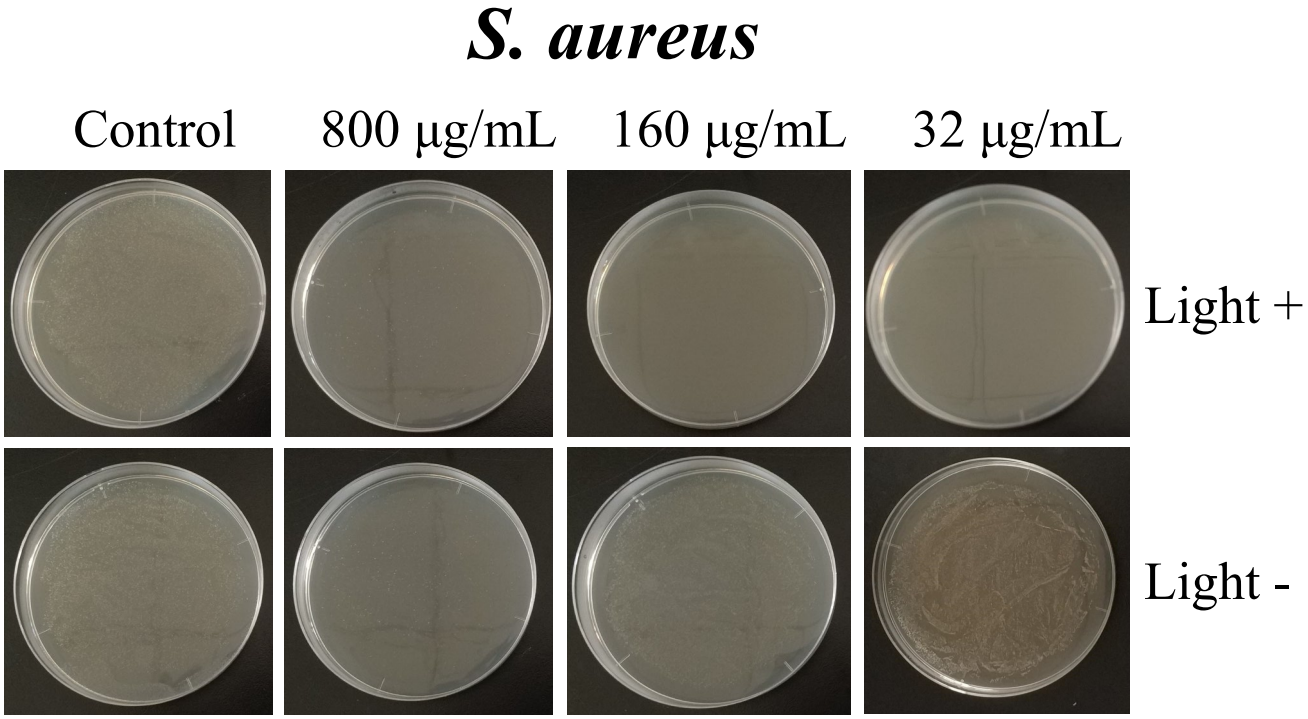

Figure S6. Photoscopic images of *S. aureus.* Number of colony-forming units after treated with AgNP-doped LDH-Ce6 nanocomposites with and without light irradiation.

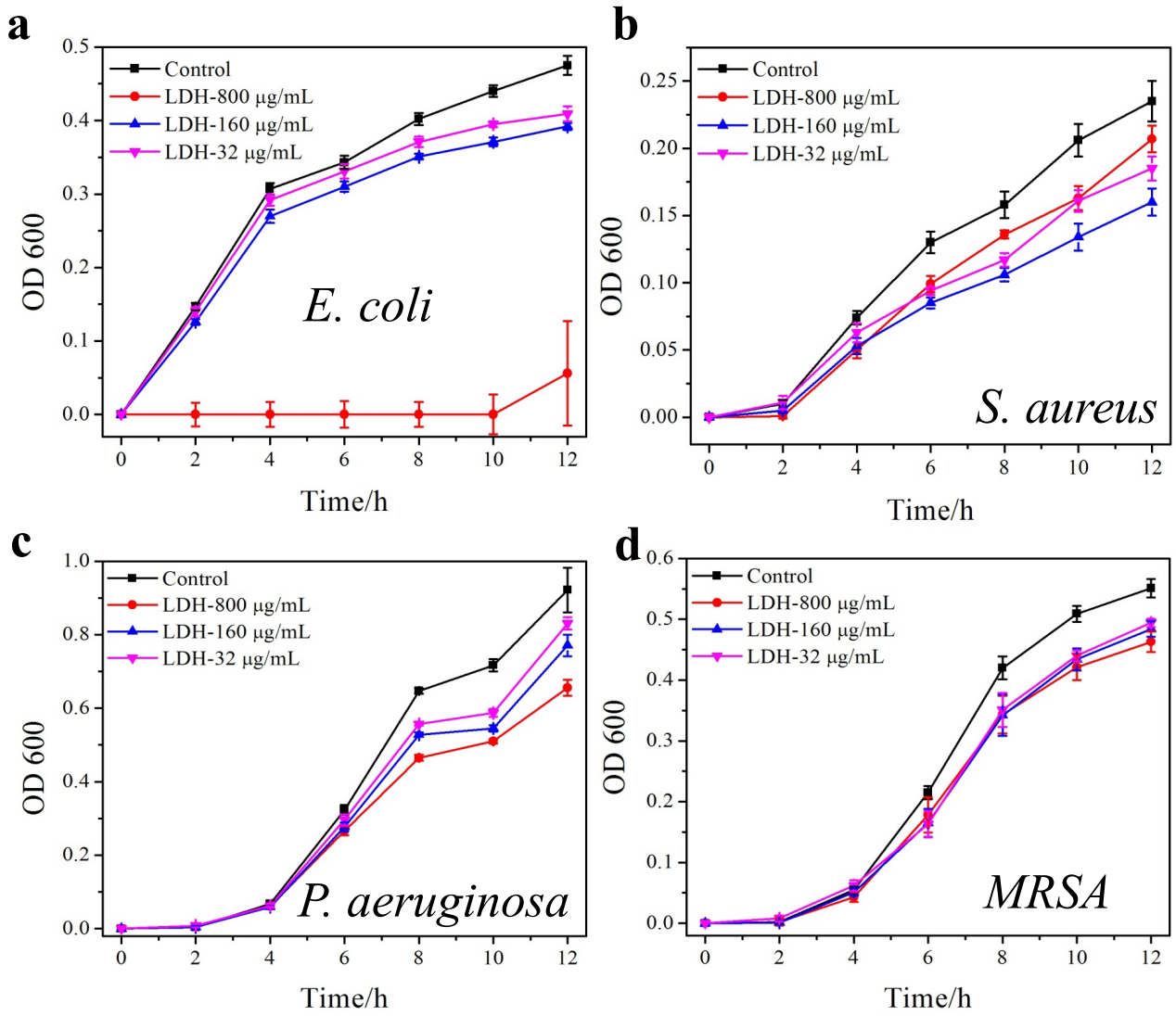

Figure S7. Bacterial inhibition analysis of conventional LDH nanoparticles. a. *E. coli*. **b.** *S. aureus*. **c.** *P. aeruginosa,* and **d.** MRSA. All data are expressed as mean ± s.d. (indicated by error bar), based on values obtained from six biological replicates (n=6).

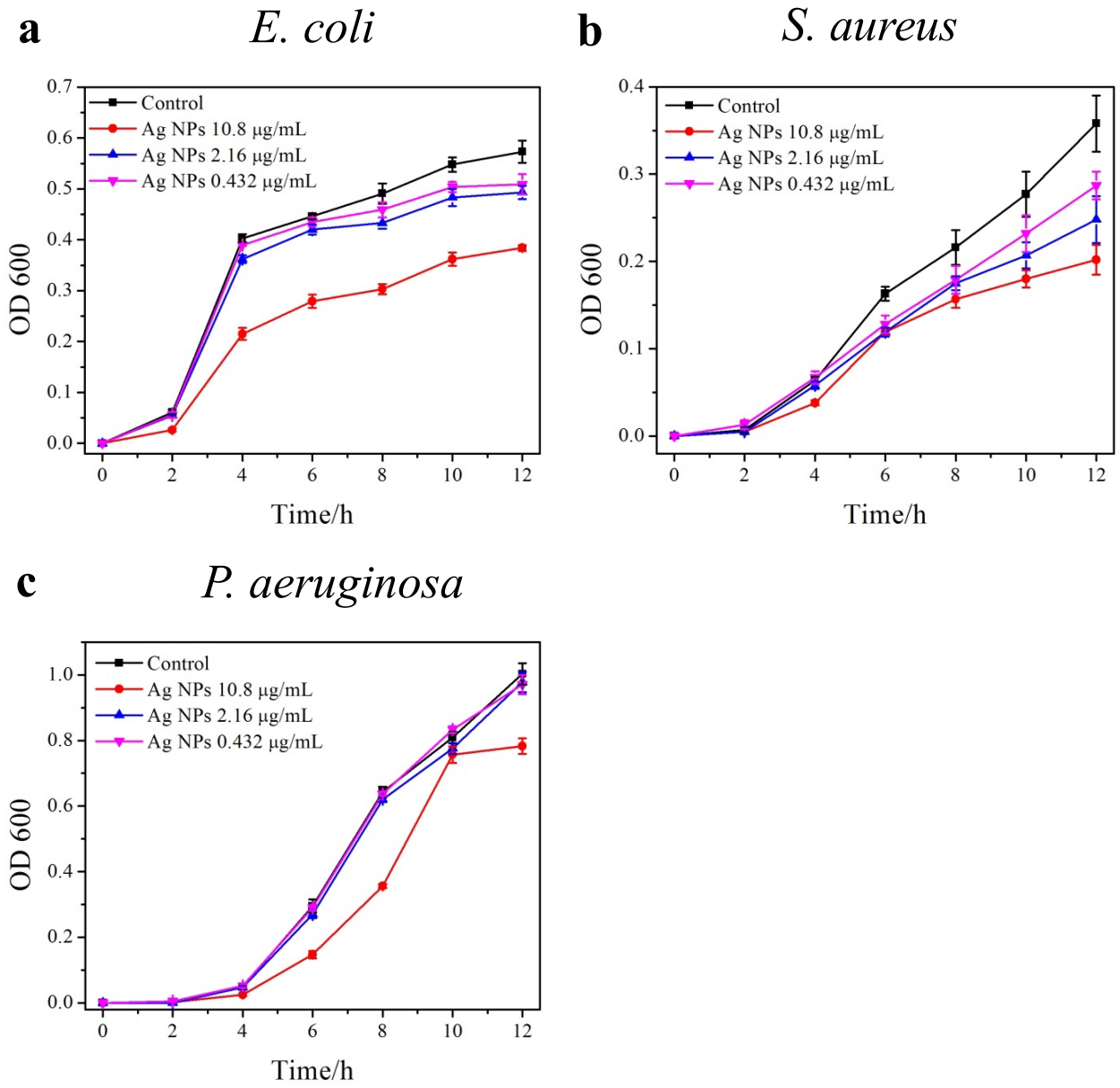

Figure S8. Bacterial inhibition analysis of conventional AgNPs. a. *E. coli*. **b.** *S. aureus,* and **c.** *P. aeruginosa*. All data are expressed as mean ± s.d. (indicated by error bar), based on values obtained from six biological replicates (n=6).